PPV-Based Conjugated Polymer Nanoparticles as a Versatile Bioimaging Probe: A Closer Look at the Inherent Optical Properties and Nanoparticle–Cell Interactions

PETERS, Martijn; ZAQUEN, Neomy; D'OLIESLAEGER, Lien; BOVE, Hannelore; VANDERZANDE, Dirk; HELLINGS, Niels; JUNKERS, Tanja & ETHIRAJAN, Anitha (2016) PPV-Based Conjugated Polymer Nanoparticles as a Versatile Bioimaging Probe: A Closer Look at the Inherent Optical Properties and Nanoparticle–Cell Interactions. In: BIOMACROMOLECULES, 17(8), p. 2562-2571.

DOI: 10.1021/acs.biomac.6b00574
Handle: http://hdl.handle.net/1942/22593

PPV Based Conjugated Polymer Nanoparticles as a Versatile Bioimaging Probe: A Closer Look at the Inherent Optical Properties and Nanoparticle-Cell Interactions

Martijn Peters†, Neomy Zaquen†, Lien D'Olieslaeger†, Hannelore Bové§, Dirk Vanderzande†⊥, Niels Hellings ‖, Thomas Junkers†⊥, Anitha Ethirajan†⊥.*

† Institute for Materials Research, Hasselt University, Martelarenlaan 42, 3500 Hasselt, Belgium.

⊥ Imec associated lab IMOMEC, Wetenschapspark 1, 3590 Diepenbeek, Belgium.

§ Biophysics and ‖ Immunology-Biochemistry, Biomedical Research Institute, Hasselt University, Agoralaan Building C, 3590 Diepenbeek, Belgium.

ABSTRACT

Conjugated polymers have attracted significant interest in the bioimaging field due to their excellent optical properties and biocompatibility. Tailor-made poly(*p*-phenylene vinylene) (PPV) conjugated polymer nanoparticles (NPs) are in here described. Two different nanoparticle systems using poly[2-methoxy-5-(3',7'-dimethoxyoctyloxy)-1,4-phenylenevinylene] (MDMO-PPV) and a functional statistical copolymer 2-(5'-methoxycarbonylpentyloxy)-5-methoxy-1,4-phenylenevinylene (CPM-MDMO-PPV), containing ester groups on the alkoxy side chains, were synthesized by combining miniemulsion and solvent evaporation processes. The hydrolysis of ester groups into carboxylic acid groups on the CPM-MDMO-PPV NPs surface allows for biomolecule conjugation. The NPs exhibited excellent optical properties with a high fluorescent brightness and photostability. The NPs were *in vitro* tested as potential fluorescent nanoprobes for studying cell populations within the central nervous system. The cell studies demonstrated biocompatibility and surface charge dependent cellular uptake of the NPs. This study highlights that PPV-derivative based particles are a promising bioimaging probe and can cater potential applications in the field of nanomedicine.

KEYWORDS : Conjugated Polymers, Fluorescent Nanoparticles, PPV, Cell-Nanoparticle Interactions, Central Nervous System, Bioimaging

INTRODUCTION

The tremendous efforts taken in understanding biological processes at the molecular and cellular level have led to great advances in the development of imaging tools as well as imaging probes in the last decades.[1-3] In this regard, optical imaging using fluorescence-based techniques has seen a steep rise in development leading to an unprecedented level of spatial resolution and temporal imaging that allows for investigation of biological activities such as protein transport, regulatory pathways and gene expression.[4-7] However, the potential of these advanced methods greatly depends on the characteristics of the fluorophore used as these significantly influence the detection limit, sensitivity and reproducibility of the employed technique.

Despite their extensive use, traditional probes like organic fluorophores, are hindered in high sensitivity cellular imaging applications owing to their low intensity, tendency to photobleach and a fast cellular clearance.[8-9] Encapsulation in suitable inorganic/polymeric nanocarriers can counter some of these problems. However, problems associated with the physical characteristics of the employed materials and dye can lead to detrimental effects such as self-quenching as well as exclusion of the dye leading to erroneous interpretations and toxicity related issues.[10-12] Another prominent example under active development are colloidal inorganic semiconductor nanoparticles (NPs), also known as quantum dots, which in comparison hold several advantages such as resistance to photobleaching and a size and composition dependent narrow emission.[13] However, their potential as biological labels is still under debate due to *in vivo* degradation and both short as well as long-term cytotoxicity issues.[14] With the above-mentioned classes of materials, significant advances have been made whereby an exciting array of alternatives has

become available. Yet, given the number of remaining limitations, the search for new *in vitro* and *in vivo* fluorescence probes remains ongoing.

In this regard, a very promising class of fluorescent nanoprobes is water-based luminescent nanoparticles formulated using conjugated polymers. With the inherent conjugated backbone, the latter have stipulated large interest outside the field of flexible electronics due to their excellent optical properties – fluorescence brightness, ideal photostability, fast radiative rate and nonblinking behavior – together with biocompatibility for use in the bioimaging field.[15-17] Among the different polymers poly(*p*-phenylene vinylene) (PPV), a pioneer material for the first organic light emitting diode (oLED) and since then one of the most thoroughly studied conjugated polymers, is of great interest owing to its reliable synthesis routes in combination with design flexibility offered by the recent control methodologies for realizing tailor-made functional PPVs, simple scale up potential and their well-known photophysical properties.[18-20]

Though PPV derivatives are highly interesting as a fluorophore, their interaction with biological environments and performance as bioimaging probe have not yet been fully explored to date, the research emphasis laying predominantly on synthesis routes and inherent material characteristics. Only the use of poly[2-methoxy-5-(2-ethylhexyloxy)-1,4-phenylenevinylene] (MEH-PPV) and poly[2,5-dicyano-*p*-phenylene vinylene] (CN-PPV) for biomedical applications has been studied more extensively, but these specific PPVs lack the functional groups necessary for surface modification when formulated for more advanced applications.[21-24] Functional moieties on the NP surface play an important role since they determine their biological identity.[25-26] They are indispensable for attaching biomolecules to impart for instance target specificity or a stealth

effect. Instead of being forced to use complex and tedious post-synthesis methods in a later stadium or surface adsorbed surfactant molecules[15], functionalized PPVs synthesized via the sulfinyl precursor route offer an elegant alternative to introduce surface functional groups. By employing such custom-made PPV-derivatives for the NP formulation, the synthetic identity of the NP based bioimaging probe can be fine-tuned to meet the set out conditions in the biological environment.

This study aims to shed light on the inherent characteristics of these yet unexplored PPV-based NPs, as compared with other established probes, and their interaction with biological systems resulting in a more profound insight in the use of conjugated polymer nanoparticles in biological sciences. The hydrophobic polymers are formulated into water-based NPs using the versatile miniemulsion technique in combination with the solvent evaporation method (**Figure 1**A).[27-28] Briefly, a two phase system is created consisting of a dispersed phase, containing preformed conjugated polymer dissolved in chloroform, an easy to evaporate organic solvent and a continuous phase, containing surfactant in an aqueous solution.[29] After emulsification using high shear forces, stable nanodroplets are generated in which – after evaporation of the solvent – solid nanoparticles are formulated by precipitation of the conjugated polymer chains. In this way, a homogenous population of stable nanoparticles is created with a size range ideal for biomedical applications.[30-31] In here, two separate nanoparticle systems are designed using poly[2-methoxy-5-(3',7'-dimethoxyoctyloxy)-1,4-phenylenevinylene] (MDMO-PPV) and a functional statistical copolymer 2-(5'-methoxycarbonylpentyloxy)-5-methoxy-1,4-phenylenevinylene (CPM-PPV-co-MDMO-PPV, for simplicity henceforth CPM-MDMO-PPV) containing ester groups on the alkoxy side chains (**Figure 1**B and C). The ester groups present on the surface of the CPM-

MDMO-PPV NPs can be conveniently converted into carboxylic acid groups through hydrolysis for the facile coupling of various biomolecules as per demand. As a proof-of-concept, in here gold-labeled antibodies (Ab) were attached to the NP surface. As finding therapies for central nervous system (CNS) diseases is often a stumbling block due to the complexity involved in the underlying biological processes, it is imperative to understand the biological activities occurring at the cellular level. Therefore, there is a significant interest for potential imaging probes for studying CNS processes.[32] In the present study, conjugated polymer nanoparticles as a suitable fluorescent nanoprobe for studying cell populations within the CNS was tested. To date and to the best of our knowledge such studies do not exist for PPV-based NPs and in general only very limited studies involving conjugated polymer NPs for such biological systems are available.[33]

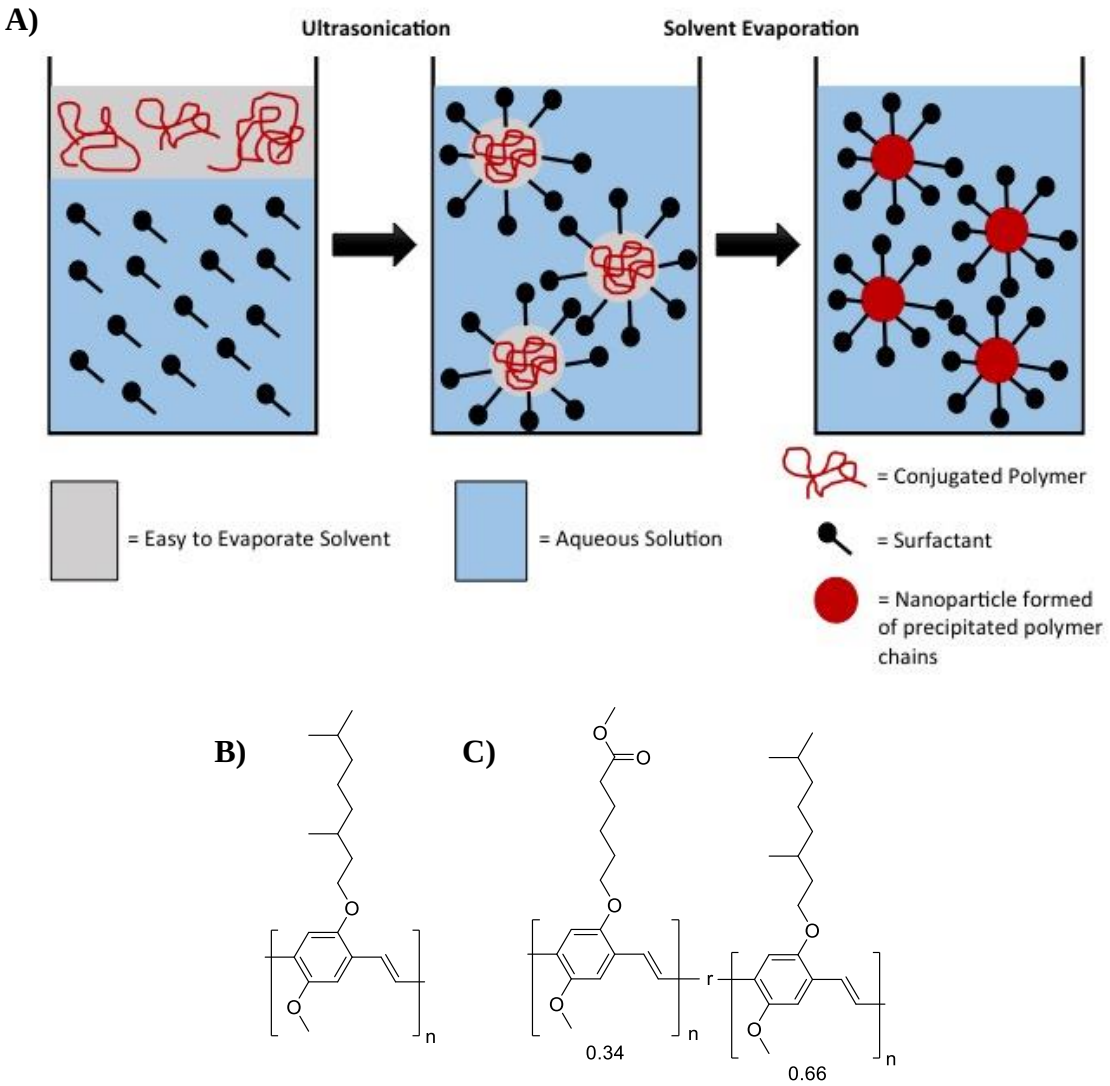

Figure 1. Combination of the miniemulsion technique and solvent evaporation method for the synthesis of conjugated polymer nanoparticles (A) and chemical structure of the used PPV-derivatives: MDMO-PPV (B) and CPM-PPV-*co*-MDMO-PPV (34:66 copolymer ratio) (C).

EXPERIMENTAL SECTION

Materials

Sodium dodecyl sulfate (SDS), amicon ultra filter membrane tubes, 1-ethyl-3-(3-dimethylaminopropyl)carbodiimide (EDC) and sucrose were purchased from Merck (Overijse, Belgium). MDMO-PPV and CPM-PPV-*co*-MDMO-PPV were synthesized using the sulfinyl precursor route.[34-35] The gold-labeled goat anti-mouse IgG(H+L) was purchased from KPL (Erembodegem, Belgium). Triton X-100 was purchased from Sigma-Aldrich (Diegem, Belgium) as well as tetrahydrofuran (THF), deuterated chloroform ($CDCl_3$), rhodamine 6G, rhodamine B, fluorescein isothiocyanate (FITC), hydrogen peroxide (H_2O_2), penicillin/streptomycin (P/S), hydrocortisone (HC), L-glutamine, trypsine and paraformaldehyde (PFA). Chloroform ($CHCl_3$) and sulfo-N-hydroxysulfosuccinimide (NHS) were bought at VWR (Leuven, Belgium). The square-mesh copper transmission electron microscopy (TEM) grids were bought from Electron Microscopy Sciences (Hatfield PA, US). MCDB 131 medium, Dulbecco's Modified Eagle Medium (DMEM) medium, Iscove's Modified Dulbecco's Medium (IMDM) medium, fetal calf serum (FCS), recombinant human epidermal growth factor (EGF), methylthiazolyldiphenyl-tetrazolium bromide (MTT), alamar blue, mouse monoclonal anti-α-tubulin antibody, Alexa Fluor® 488 Donkey Anti-Mouse IgG (H+L) antibody and 4',6-Diamidino-2-Phenylindole (DAPI) were purchased from Life Technologies (Ghent, Belgium). Bovine serum Albumin (BSA) was bought at USBiological (Swampscott MA, US). The culture plates and dark plates were obtained at Greiner Bio One (Vilvoorde, Belgium). The µ-Slide 8 Well plates were ordered at Ibidi. The 1x phosphate buffered saline (1xPBS) was bought at Lonza (Verviers, Belgium). HeLa (CCL-2), C8-D1A cell line (CRL-2541) and human microvascular endothelial cells (HMEC)-1 (CRL-3243) were purchased at ATCC (Molsheim, France). BV-2 cell line

(ATL03001) was bought at ICLC (Genova, Italy). All chemicals were used as provided without further purification.

PPV-Based Nanoparticle Preparation

Conjugated polymer nanoparticles using MDMO-PPV and the statistical copolymer CPM-MDMO-PPV were synthesized using the combination of miniemulsion and solvent evaporation method. Both PPV derivatives and their respective monomers were synthesized following literature procedures.[34-35] A solution of MDMO sulfinyl premonomer (1.00 g, 2.05 mmol, 0.30 equiv.) and CPM sulfinyl premonomer (2.27 g, 4.77 mmol, 0.7 equiv.) in *sec*-butanol (14.8 mL) and a base solution of Na*t*BuO (0.256 g, 2.67 mmol, 1.3 equiv. to 1 equiv. premonomer blend) in *sec*-butanol (16.8 mL) were degassed three times at 30 °C using nitrogen. Equivalents (0.3 and 0.7) represent the theoretical ratio of the monomer units within the copolymer. In case of MDMO-PPV polymer synthesis only 1 equiv. of MDMO sulfinyl premonomer is taken. The base solution was added in one portion to the stirred monomer solution to start the reaction. After 1 h, the reaction was quenched with HCl (1 M, 50.0 mL). After extraction with CH_2Cl_2 (3 mL × 50 mL) and evaporation, synthesis towards the conjugated PPV was immediately followed. Precursor PPV (2.00 g) in toluene (200 mL) was degassed by purging for 15 min with nitrogen, after which the solution was heated to 110 °C and stirred for 3 h under nitrogen atmosphere. Subsequently, the reaction was cooled down to room temperature and precipitated in cold MeOH (40 mL) and filtered on a Teflon® filter. This enables to selectively isolate the desired high-molecular weight polymer product (gravimetric yield 75 %). The conjugated CPM-MDMO-PPV as well as the MDMO-PPV polymer were obtained as a red solid. The obtained MDMO-PPV

polymer had a molecular weight (M_n) = 150 000 g·mol^{-1} with dispersity ($Đ$) = 2.7 and the CPM-MDMO-PPV polymer a M_n = 164 200 g·mol^{-1} with $Đ$ = 2.7.

For the NP formulation, the continuous phase consisted of 16 g from a 72 mg SDS in 24 g ultrapure water solution. The dispersed phase contained 100 mg of the respective conjugated polymer in 6.625 g of $CHCl_3$. After adding the continuous phase to the dispersed one, the mixture was pre-emulsified for 1 hour at 1000 revolutions per minute (rpm) at room temperature. The pre-emulsification step was followed by ultrasonication under ice cooling using a Branson 450W digital sonifier (Soest, The Netherlands) with a 1/4"-tip for 3 min at 65 % amplitude using a 30 s pulse and 20 s pause regime. The resulting nanodroplet containing emulsion was placed on a hotplate and the organic solvent was evaporated at 40 °C by stirring for 18 h at 500 rpm. The resulting red colored dispersion was passed through a paper filter (Whatman, pore size 4 – 7 µm) to remove any large aggregates. The excess SDS was washed using multiple centrifugation/redispersion steps with a Sigma 3-30K centrifuge (Suarlée, Belgium). First, 40 washing steps of 30 min at 2000 rpm were done with membrane tubes, followed by 3 steps at 14 000 rpm for 1 h with eps. The washed sample, was stored in the dark and used as required. The nanoparticles samples were always sterilized with 30 Gy (= 3000 rad) using an IBL 437C type gamma radiator, Cis Bio International (Codolet, France), before usage in cell experiments.

For coupling gold-labeled Ab, CPM-MDMO-PPV NPs were diluted to a solid content of 0.005% with a total solution volume of 3 mL. A 1 mL solution containing 0.025 mg EDC and a 1 mL solution containing 0.014 mg sulfo-NHS were added to the NP solution. The resulting sample solution was stirred for 20 min at 750 rpm in the dark after which 200 µL of the gold labeled

goat anti-mouse IgG solution was added. The sample was stirred for an additional 3 h at 750 rpm in the dark followed by washing using 3 cycles of centrifugation (14 000 rpm, 45 min) and redispersion steps.

Cell Culture

Cells were cultured with culture medium (**Table 1**) in a T25 flask stored at 37 °C in a 5% CO_2 incubator (Sanyo, Japan) and were spliced after being 80% confluent. For HMEC-1 cells, the medium needs to be refreshed after 3 days.

Table 1. Cell-lines and respective culture media.

Cell type	Medium	Supplements
HMEC-1	MCDB 131	10 % FCS
		0.5% P/S
		500 ng EGF
		50 µg HC
		500 µmol L-Glutamine
BV-2	DMEM	1 % P/S
		10 % FCS
C8-D1A	DMEM	1 % P/S
		10 % FCS

Cytotoxicity Assays

Alamar blue assay. HeLa, HMEC-1, BV-2 and C8-D1A cells were seeded in a 96-well flat bottom plate and left to grow to 80% confluence at 37 °C in a 5% CO_2 incubator. The desired sample concentration range (5, 10, 50 and 100 µg/mL) was obtained by diluting the sample with phenol red poor IMDM culture medium (replacing the medium solution of **Table 1** in the culture medium) and 100 µL of each concentration was added to the wells after washing with 1xPBS (9 g/L NaCl, 0.795 g/L Na_2HPO_4 and 0.144 g/L KH_2PO_4). Also positive and negative control conditions were included. A total of six wells was taken per condition. After a 24 h at 37 °C, the conditions were removed and the cells were washed 3 times with 1xPBS. Then a 10 % alamar blue solution in IMDM culture medium was added and left to incubate for 24 h. The resulting solution was transferred to an opaque-walled dark 96-well culture plate and the fluorescence was measured at λ_{em} = 590 nm while excited at λ_{ex} = 570 nm, FLUOstar OPTIMA (BMG Labtech, Temse, Belgium). The experiment was performed in triplicate.

Uptake Kinetics

HMEC-1 cells were seeded at a density of 100 000 cells per well in a 24-well plate and left to incubate for 24 h at 37 °C and 5% CO_2. Subsequently, the cells were washed with 1xPBS and 500 µL of 75, 100, 150 and 200 µg/mL of NPs in culture solution was added to the cells which were then incubated for 2, 4, 6, 8, 24, 27 or 30 h at 37°C with a CO_2 level of 5%. The cells were washed 3 times with 1xPBS and harvested. The pellet was dispersed in 1 mL of 4% PFA and left to incubate for 20 min at room temperature in the dark. The cells were then centrifuged in order to remove the PFA solution and washed 3 times using centrifugation with fluoresence-activated cell sorting (FACS) buffer (1xPBS and 2% FCS). The resulting samples were measured and

analyzed with the FACSCalibur, Becton Dickinson (Erembodegem, Belgium), using a 488 nm laser and an emission filter 585/42 nm. Unlabeled cells were used as a blank to gate the signal. For each sample 20 000 cells were counted in triplicate. The FACSCalibur software counted and calculated the amount of cells in the cell culture solution and measured in which cells fluorescent signal was detected. These calculations were converted to a percentage scale, with 100% meaning that in all measured cells fluorescence, and thus NPs, was detected.

Confocal Laser Scanning Microscopy

HMEC-1, BV-2 and C8-D1A cells were seeded in a µ-Slide 8-well plate (Ibidi) at a concentration of 50 000 cells per well and left to adhere and grow for 12 h at 37 °C. The cells were washed with 1xPBS after which 50 µg/mL of MDMO-PPV NPs and CPM-MDMO-PPV NPs in IMDM culture medium was added to each well and incubated for 20h. The cells were washed 3 times with 1xPBS and 100 µL of IMDM culture solution was added. All images were collected at 37 °C using a Zeiss (Zaventem, Belgium) LSM510 META NLO mounted on an inverted laser scanning microscope (Zeiss Axiovert 200 M) and a 40x/1.1 water immersion objective. Excitation of the nanoparticles was done at 488 nm (3 µW maximum radiant power at the sample) with the Argon-ion laser. Emission was detected using a band-pass filter of 565-615 nm. The resulting 1024x1024 images with a pixel size of 0.06 µm were recorded using a pixel dwell time of 14.2 µs. A fixed pinhole size of 114 µm was used. Images were processed using AIM 4.2 and ImageJ software.

RESULTS & DISCUSSION

Synthesis of Nanoparticles using PPV Derivatives

Conjugated polymer nanoparticles were obtained from MDMO-PPV (M_n = 150 000 g·mol^{-1}) or statistical co-polymer CPM-MDMO-PPV (M_n = 164 200 g·mol^{-1}, 66:34 MDMO:CPM ratio as determined by ^{1}H NMR, FTIR peak of ester at 1730 cm^{-1})[36] to serve as bioimaging probes (Figure S1-4). Both PPVs were synthesized *via* the so-called precursor sulfinyl route.[34-35] Next to a very fast polymerization and high conversion being reached within a second to minute time scale, this specific route differs from others in its use of an unsymmetrical premonomer which results in better control over the regioregularity as compared to for instance, the Gilch route.[35] In addition to this, the sulfinyl precursor route enables the design of complex polar functionalized PPVs, as CPM-MDMO-PPV, in an easy manner. Subsequently, the polar group on the side chain can be substituted for a sheer unlimited number of chemical functionalities, such as propargyl groups that are highly interesting to perform orthogonal conjugation reactions (also known as "click reaction") using dicyclohexylcarbodiimide/4-dimethylaminopyridine (DCC/DMAP) post-polymerization functionalization.[34, 36] As the CPM-MDMO-PPV bears ester groups on the alkoxy side chain, the formulated NPs are expected to have the ester groups distributed within the volume and on the surface of NPs. The ester groups present on the surface of the CPM-MDMO-PPV NPs can be conveniently converted into carboxylic acid groups, using hydrolysis, which can subsequently be employed for the easy attachment of various biomolecules for incorporating different functional properties (*e.g.*, induce target specificity, enhanced circulation time, barrier crossing potential, or others). It should be noted that direct polymerization of an acid-functionalized monomer is impossible due to the basic nature of any precursor polymerization technique leading to PPVs.

The particle formulation using both preformed polymers was performed using a combination of the solvent evaporation and miniemulsion technique, which allows for generating nanoparticles with tunable size, surface functionality and also dispersions with tunable solid content depending on the polymer amount used.[28] The characteristics of the two different particle systems are presented in **Table 2**.

Table 2. *Characteristics of the synthesized PPV-based nanoparticles (Mean ± SD)*

Formulation		**Characteristics**			
		TEM (nm)	**DLS (nm)**	**Zeta potential (mV)**	**Solid content (%)**
NP 1	(MDMO-PPV)	97 (±10.0)	116(±1.8; PDI = 0.060)	-29.8	1.1
NP 2	(CPM-MDMO-PPV)	84(± 11.7)	117 (±1.8; PDI = 0.063)	- 41.9	0.8

The solid content values reported here represent the values obtained immediately after synthesis and before the required washing steps to remove the excess of SDS. As it can be seen in **Table 2**, the obtained average hydrodynamic diameter values deduced from dynamic light scattering (DLS) are in the same range with narrow polydispersity indices (PDI) for both NPs. As the size of the particles does not vary, it can be inferred that the type of used polymer does not significantly influence the particle formation in the present case. The more negative zeta potential value for the CPM-MDMO-PPV NPs (-41.9 mV) compared to the MDMO-PPV NPs (-29.8 mV) indicates that some of the ester groups have already been hydrolyzed during the washing steps to form carboxylic acid groups. With transmission electron microscopy (TEM) the average size of the actual conjugated polymer core was determined. These results indicate

slightly smaller diameters than DLS, as expected as the latter measures the hydrodynamic radius. The TEM image (**Figure 2** and S5) also highlights the spherical morphology of the synthesized nanoparticles. Further, it is also shown that after extensive washing, a colloidally stable colored dispersion is obtained (**Figure 2**).

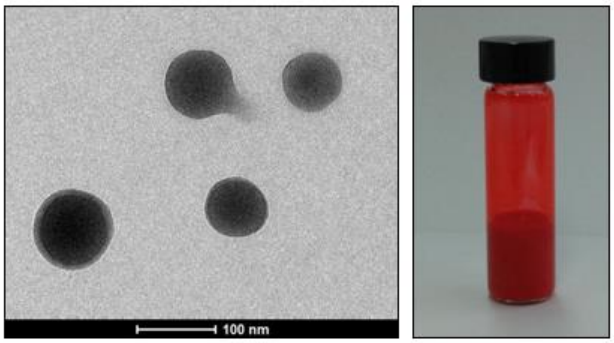

Figure 2. TEM image of CPM-MDMO-PPV NPs (*left*) and a photograph of stable water-based NP dispersion (*right*).

As previously mentioned, surface functionalization of NPs is an inevitable requirement in nanomedicine. Therefore, as a proof of concept to demonstrate the ease of attaching biological moieties onto the surface when using the surface carboxylic acid containing CPM-MDMO-PPV NPs, gold-labeled goat anti-mouse IgG Ab were attached using EDC-coupling.[37] The presence of these gold-labeled Ab was proven visually using TEM imaging and confirmed using energy-dispersive x-ray (EDX) (Figure 3 and S6). The difference in contrast due to the higher electron density of the gold NPs as compared to the polymer particles, clearly enables to visualize the presence of gold-labeled Ab. It can be seen that multiple darker spots (gold NPs) are present on the polymer particle after washing steps thereby confirming the former's firm covalent attachment. Since a multiple centrifugation and dispersion protocol, involving mechanical forces, was adopted for washing the NPs after the coupling reaction, some of the gold-labeled Ab were

detached as is also seen in the TEM image. EDX analysis shows characteristic peaks of gold (2.1 and 9.7 keV), while the peaks of copper can be attributed to the grid on which the sample is placed.[38]

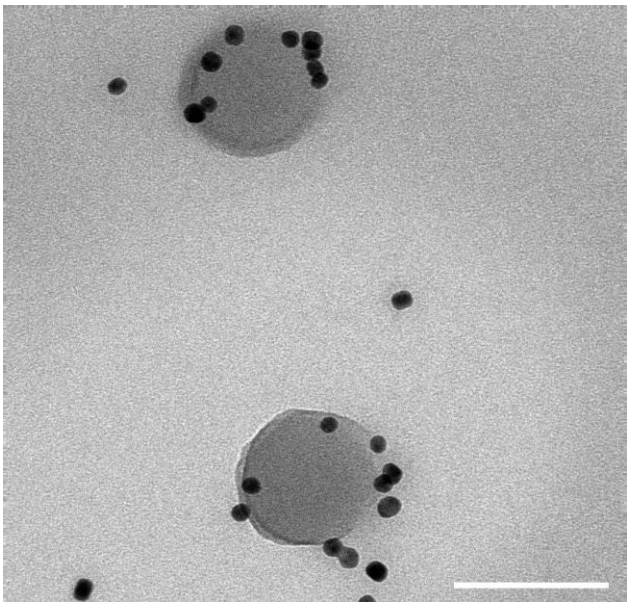

Figure 3. TEM image of CPM-MDMO-PPV NPs functionalized with gold labeled Ab. Scale bar represents 100 nm.

Optical Characteristics of a PPV-Derivative Based Bioimaging Probe

The optical properties of the NPs were studied in detail using different optical spectroscopic techniques. UV-Vis and fluorescence spectroscopy were used to measure the absorbance and emission spectrum of both molecularly dissolved MDMO-PPV and CPM-MDMO-PPV chains in chloroform and their respective NPs in water (**Figure 4**). A feature characteristic of conjugated polymer nanoparticles is their broad absorption band ranging from 350 to 600 nm. This large wavelength range is ideal for applications like fluorescence microscopy. The absorption spectra of the nanoparticles are broadened as compared to that of the free chains, caused by the torsion, kinking and bending of the polymer backbone.[39] Also a clear shift in the emission maximum

peak was observed from 550 to 590 nm when going from molecularly dissolved chains to NP configuration. This can be attributed to the change from intrachain emission to interchain emission when the conjugated polymers aggregate, during the evaporation of the solvent, into nanoparticles.[39] The occurring red shift is caused by overlap of π-orbitals during aggregation, which leads to a delocalization of the π-electrons across several chains causing the formation of new electronic species with lower band gaps.[39-40] Also, a lower energy shoulder becomes visible, corresponding to the relaxation of π-electrons through a ground state energy level.[41]

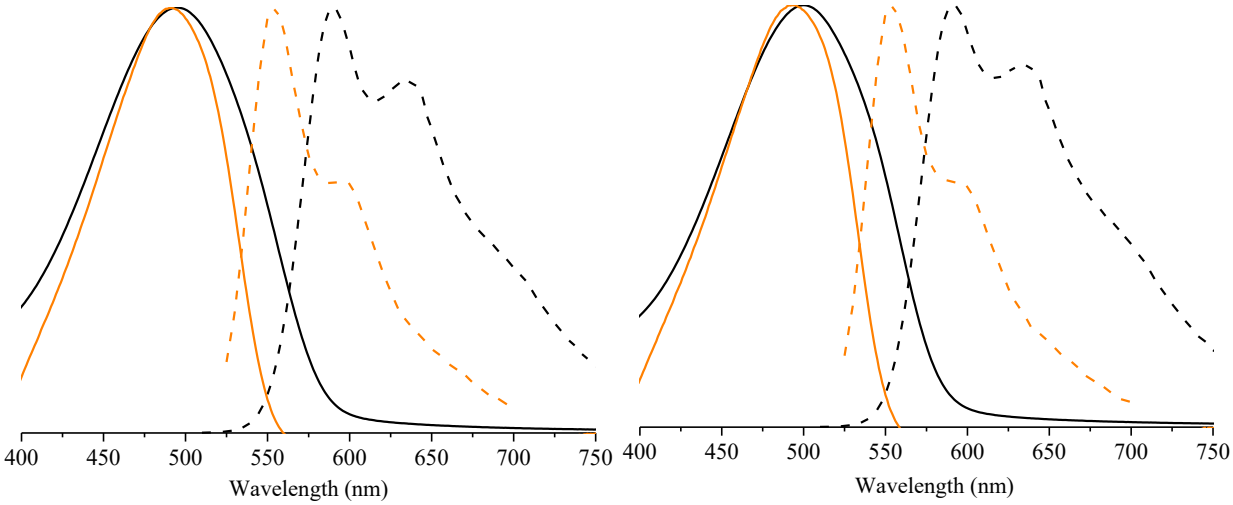

Figure 4. Optical spectra (*absorbance solid and emission dashed line*) of MDMO-PPV (*left*) and CPM-MDMO-PPV (*right*) in different forms: molecularly dissolved polymer in chloroform (*orange*) and NPs in water (*black*).

Recently multiphoton microscopy has emerged as a powerful technique for 3-D imaging in biological systems.[42-43] In two-photon fluorescence, two photons are absorbed simultaneously by the imaging probe under investigation to promote an electron to its excited state. When the electron relaxes back to its ground state level, it emits a photon identical to one-photon absorption and fluorescence. In this manner a highly localized excitation and improved spatial resolution is generated caused by the nonlinear dependence of excitation probability on light

intensity.[43] In addition, the background signal caused by autofluorescence and fluorescence outside the focal plane is greatly reduced by the small effective excitation volume.[43] The ability to employ near-IR wavelengths during excitation reduces the photodamage to the sample as well as photobleaching to the probe, facilitates deep tissue imaging (up to 1 mm) resulting from the near-transparency of a wide range of tissues and biological water in the used spectral range and enables an enhanced image quality due to a decrease in light scattering by for example cells.[43] It has been demonstrated that conjugated polymers possess a larger efficiency when it comes to multiphoton absorption as compared to conventional dyes.[42, 44] Therefore, the two-photon excitation and emission characteristics of the constructed PPV-based NPs were also studied (Figure 5). For both MDMO-PPV NPs and CPM-MDMO-PPV NPs the excitation maximum was located at a wavelength of 830 nm. The emission spectra after two-photon excitation shows features similar to the ones obtained after one-photon excitation as expected with a maximum around 580 nm for the CPM-MDMO-PPV NPs and 590 nm for the MDMO-PPV NPs.

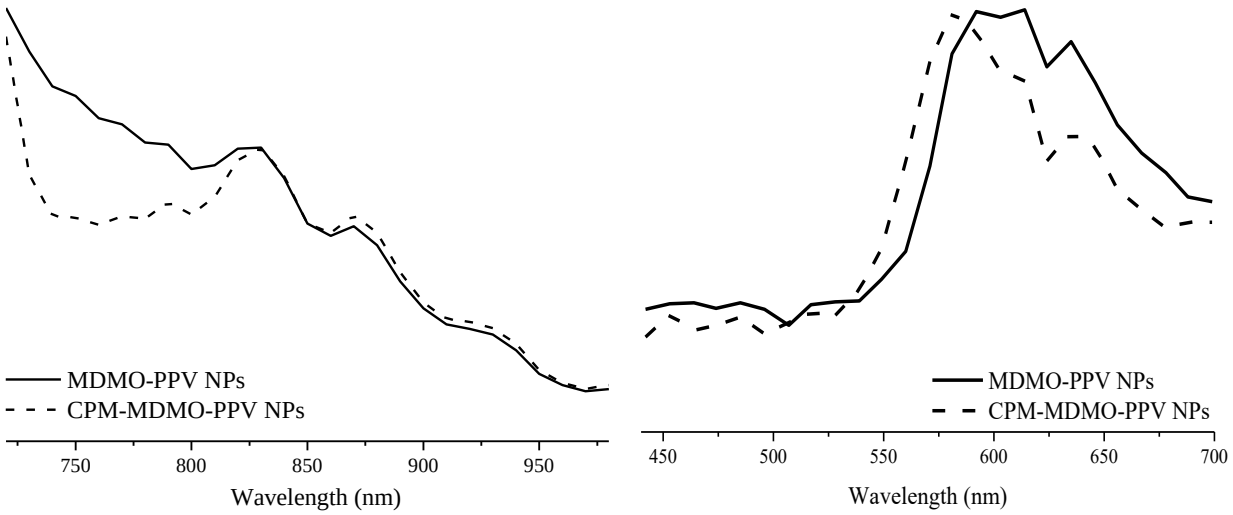

Figure 5. Two-photon fingerprint of MDMO-PPV NPs (*solid line*) and CPM-MDMO-PPV NPs (*dashed line*) with absorbance spectra on the left and emission spectra on the right.

Table 3 summarizes several inherent optical characteristics of both nanoparticle systems. A decrease in quantum yield for both NP types was observed as compared to their molecularly dissolved counterparts: from 33 % to 3 % for the MDMO-PPV NPs and from 22 % to 3 % for the CPM-MDMO-PPV NPs. It has been reported that the nanoparticle formation causes a lowering in quantum yield because of quenching, following chain confinement in the condensed phase.[39] Through the aggregation formed between the conjugated chains, exciton migration becomes more effective, resulting in excitations reaching quenching sites more easily. Therefore, this becomes a more effective relaxation path leading to a reduction in fluorescence efficiency. The NP quantum yields determined are better than the previously reported values of other PPV-based NPs, like MEH-PPV NPs of a similar size with a yield of 1 %.[8, 40, 45] Although the quantum yield of the constructed conjugated NPs is lower than those of quantum dots (0.1-0.8) and organic dyes (0.5-1.0), their molar extinction coefficients are considerably higher.[46-47] For both NP models the value is in the order of 10^6 $M^{-1}\cdot cm^{-1}$, while that of organic dyes and quantum dots is in the order of 10^5 $M^{-1}\cdot cm^{-1}$.[46-47] Consequently, the fluorescence brightness, thus the product of the quantum yield and molar extinction coefficient – in the end the determining factor for a successful imaging probe – is high. Even though not strictly required, the quantum yield can in principle be further increased through chemical structure adaptation of the conjugated polymer.[21, 48]

Table 3. Optical characteristics of the synthesized nanoparticles

	MDMO-PPV NPs	**CPM-MDMO-PPV NPs**
λ_{max} excitation (nm)	494	499
λ_{max} emission (nm)	590	590
Quantum Yield (φ_F)	3 %	3 %
Molar Extinction Coefficient (ε, $M^{-1}*cm^{-1}$)	$9.4*10^6$	$9.1*10^6$
Absorption Cross Section (σ, cm^2)	$3.60*10^{-14}$	$3.47*10^{-14}$
Lifetime (τ, ps)	518.6	418.5
Fluorescence radiative rates (K_R, s^{-1})	$6.7*10^7$	$4.8*10^7$

Fluorescence lifetime imaging microscopy (FLIM) measurements of the NPs resulted in lifetime values around 0.4-0.5 ns, similar to other PPV-based NPs but lower than organic dyes (1-10 ns) and quantum dots (10-100 ns) (Figure S7).[8, 46-47] This lifetime value is of particular importance in high-speed application like flow cytometry and high-speed tracking since it determines the fluorescence radiative rate together with the quantum yield ($\varphi = K_R/(K_R+K_{NR})$ and $\tau = (K_R+K_{NR})^{-1}$).[47] The values coincide with those reported in literature and are in the range of 10^7 s^{-1}, which is lower than the reported values of standard organic dyes (10^8 s^{-1}) and higher than those of quantum dots (10^6 s^{-1}).[8]

Another important property is the photostability of the synthesized NPs, especially if the application involves long-term imaging and tracking of NPs. After an exposure time of 1 hour the fluorescence intensity was still at 90 % integrity for the MDMO-PPV NPs and 85 % for the

CPM-MDMO-PPV NPs as compared to commonly used stable organic dyes (Figure 6.). The PPV-derivative NPs undergo little to no photobleaching. As photodegradation is a concern in such conjugated systems,[49] the NPs produced as aqueous dispersions were monitored for their optical properties over a time period of 12 months by determining the absorption integrity at different time points (Figure S8). No decrease in absorbance integrity below 90 % was observed for both MDMO-PPV and CPM-MDMO-PPV NPs as compared to the sample directly measured after synthesis and washing procedures, indicating an excellent shelf-life time of these bioimaging probes. In addition, the chemical stability was tested by measuring the integrity of absorbance after exposure to a 0.1 wt % of H_2O_2 solution, a stable and common reactive oxygen species in cells. A difference of only 0.6 % compared to the control was monitored after 24 h of exposure to this physiological environment (Figure S9).

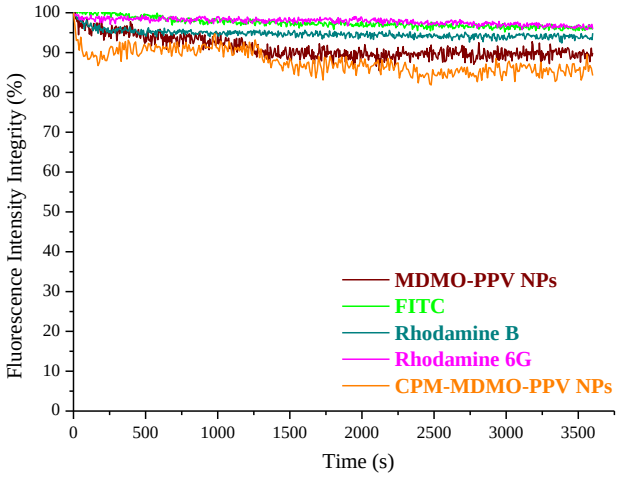

Figure 6. Photobleaching curves of organic dyes and PPV-derivative NPs.

Monitoring the Cytotoxic Behavior

Cytotoxicity of NPs is no issue for *ex vivo* applications like immunoassays, but is of great relevance for *in vitro* and especially *in vivo* applications. Therefore, the biocompatibility of

MDMO-PPV and CPM-MDMO-PPV NPs was evaluated. The results of MTT and alamar blue assays on HeLa cells showed no significant reduction ($p < 0.05$) in cell viability for any concentration of MDMO-PPV NPs as compared to the control (Figure S10-11). No concentration effect was visible ($p < 0.05$) and the observed trends were consistent between both assays.

As indicated earlier a high demand is present for bioimaging probes that can be employed for unraveling neurological diseases. Hence, the PPV-derived NPs were tested for their cytotoxicity towards different neurological cell lines associated to the brain. The viability of three different cell types incubated with increasing amounts of MDMO-PPV or CPM-MDMO-PPV NPs was assessed using the alamar blue assay (Figure 7 and Figure S12). The endothelial cell line (HMEC-1) was chosen to mimic the blood brain barrier (BBB) comprised of blood vessels which the nanoparticles have to pass, the astrocyte (C8-D1A) and microglia (BV2) cell line were chosen as representatives for the cell populations present inside the brain which the nanoparticles could encounter.

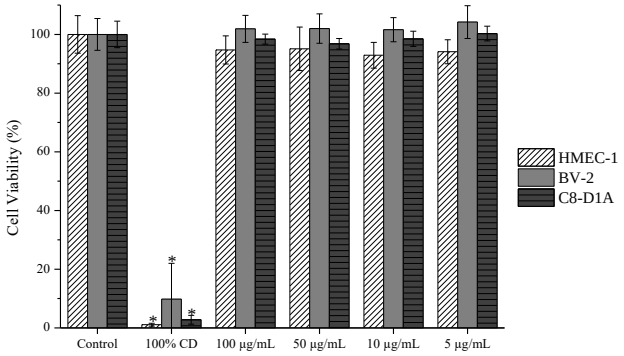

Figure 7. Dose dependent cytotoxicity of MDMO-PPV NPs after 24h of exposure determined by the alamar blue assay in HMEC-1, BV-2 and C8-D1A cells. CD = cell death. Data are expressed as percent of control mean +/- SD (N = 3).

For all three cell lines and both nanoparticle models the cell viability never went below 90 % after an exposure period of 24 h when compared to the untreated control. No statistical difference was observed between the control group and different concentrations and between the concentrations tested (one-way ANOVA $p < 0.05$). Both PPV-derivative NP systems show no significant cytotoxicity on the tested cell lines. Therefore, it can be concluded that the NPs have no discernible impact on the cell viability and no dose dependent response is present in the used concentration range.

Cellular Uptake of the PPV-derivative Based NPs

Uptake by cells as a function of time for different concentrations was studied using flow cytometry. The uptake kinetics of PPV-derivative NPs over a time period of 30 h is shown in Figure 8. The fluorescence radiative rates of the constructed NPs described earlier are high enough to be detected with flow cytometry. HMEC-1 cells of the CNS were chosen since endothelial cells make up blood vessels and are thus one of the first ones to encounter injected NPs.

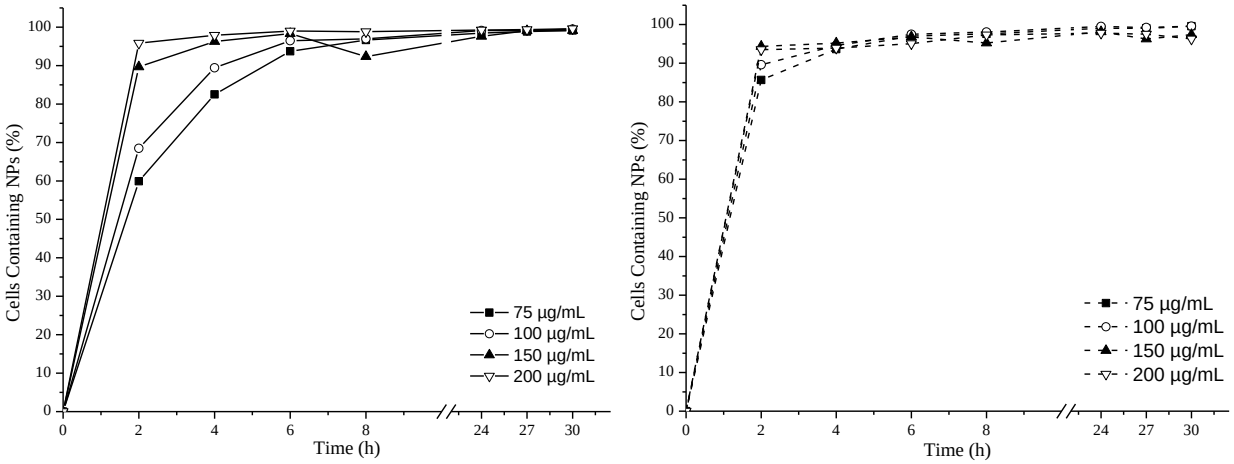

Figure 8. Kinetics of uptake: Internalization of a MDMO-PPV (*solid line*) and CPM-MDMO-PPV (*dashed line)* NP concentration range by HMEC-1 cells over a time period of 30h.

A clear difference is visible between the uptake of CPM-MDMO-PPV and MDMO-PPV NPs in the early hours. Approximately 85 % of the cells have taken up NPs after 2 hours for the lowest concentration of CPM-MDMO-PPV NPs, while this is only 60 % for MDMO-PPV NPs. When the incubation time extends, the difference fades between the two NP configurations and saturation is reached after approximately 6-8 h, meaning that all cells have taken up NPs. For high concentrations, 150 and 200 µg/mL, the discrepancy at short time periods is less pronounced. Standard deviations are not visible since they do not exceed 1.0 %. Although both particle types carry residual anionic surfactant after washing, the difference in uptake between the two configurations at lower concentrations, could be related to the presence of increased negative surface charge on the CPM-MDMO-PPV NPs due to partial hydrolysis, which occurred during the washing steps. NPs with a charge present on the surface are known to be taken up faster than NPs with no surface charge, aside from the one caused by the physically adsorbed surfactant.[50]

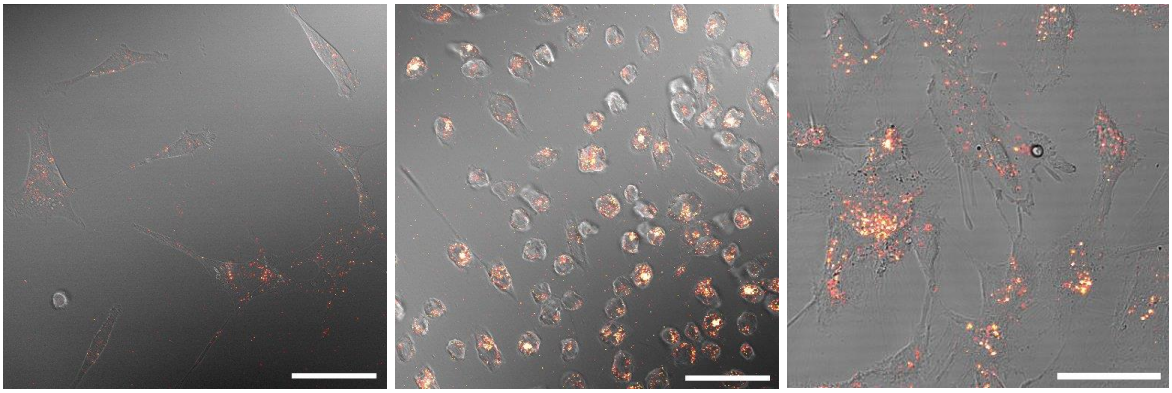

Figure 9. Confocal microscope image of C8-D1A (*left*), BV-2 cells (*middle*) and HMEC-1 cells (*right*) treated with MDMO-PPV-based NPS (*red*) for a time period of 20h. Scale bars represent 50 µm.

The uptake was also confirmed visually using confocal laser scanning microscopy (Figure 9 and Figure S13) for living HMEC-1, BV-2 and C8-D1A cells. The fluorescent NPs show to remain stable in cell culture medium and all three cell lines are taking up nanoparticles within the incubation period without any detrimental effect on the cell morphological integrity, confirming the results of the cytotoxicity measurements.

The astrocytes show rather flat polygonal fibroblast-like cell bodies (type 1) instead of central neuron-like bodies with long thing protrusions (type 2) (Figure S14).[51] This is not due to the NP incubation but because C8-D1A cell lines belong to the type 1 astrocytes subcategory, as most culture cell lines do.[52] The C8-D1A cell line was chosen since it is used most frequently to study *in vitro* the astrocyte properties and are more associated with the blood brain barrier than other types of astrocytes, thus having a higher probability of encountering the incorporated nanoparticles.[52]

A larger uptake of NPs is seen in the BV-2 cells compared to the HMEC-1 and C8-D1A cells, which can be explained by the nature of the cells. The murine BV2 cell line is made through infecting primary microglial cell cultures with a v-raf/v-mvc recombinant retrovirus, exhibiting phenotypic as well as functional properties of active microglial cells and is widely employed in neuroscience research.[53] Microglial cells are immunocompetent macrophage-like cells, comprising 20 % of the total glial cell population, that are forming the core of the immune system inside the central nervous system.[54] Their role is to form the first line defense of the brain against invasions of foreign microorganisms, thus they are most likely the first ones to respond to NPs.[55] Normally they have a ramified structure with small protrusions, but when activated this

changes to an amoeboid-like appearance in order to migrate to the required site and phagocytize the intruders.[56] The larger uptake is thus correlated to the uptake mechanism of this specialized cell which is phagocytosis.[50] No ramified structure was seen on the confocal images, but it is documented that microglial cells do not have this feature *in vitro* and show rather heterogeneous shapes like spindles, rods or even round which is the case in the confocal images.[57] Since the NPs are not covered with any biological agents, which could provide stealth, they activate and are taken up in large numbers by the microglia, hence explaining the uptake difference with HMEC-1 and C8-D1A cells. Amoeboid-like appearances as well as pseudopodia used to engulf and take up the nanoparticles can be visualized in Figure S15. It should be noted that the BV-2 cells were not stimulated by pharmacological agents, like macrophage colony stimulating factor (rM-CSF), used to induce phagocytosis or micropinocytosis.[58] All observations of the behavior of the cells regarding NP uptake in physiological conditions can thus be regarded as spontaneous. Apart from the neurological cell lines, HeLa cells also showed uptake of NPs as can be seen in Figure S16. Internalization of the NPs was confirmed by z-stacks throughout the cells (see video of image series acquired for HeLa cell after 24 h incubation).

CONCLUSION

MDMO-PPV and CPM-MDMO-PPV NPs with a 100 nm size range were synthesized using the combination of miniemulsion and solvent-evaporation method. A more negative zeta potential was observed for the CPM-MDMO-PPV NPs, caused by carboxylic acid groups on the alkyl side chain. The latter renders the NP surface with functional groups that can be used for biomolecule conjugation. As a proof of principle, gold-labeled Ab were successfully attached to the NP surface. The study of optical properties revealed that the polymer in the nanoparticle configuration exhibited different characteristics as compared to their respective molecularly dissolved counterparts. Optical properties studies of the NPs determined a fingerprint of 500/590 nm. A clear shift from 550 to 590 nm in the emission maximum was observed for the NPs. This can be attributed to the characteristic switch from intrachain emission to interchain emission. Both NPs exhibit excellent photostability as no photobleaching occurred after 1 h of continuous exposure, compared to reference dyes. A quantum yield of 2-3 % was observed combined with a high molar extinction coefficient of $9*10^6\ M^{-1}\cdot cm^{-1}$, resulting in a high fluorescence brightness. The NPs excited state lifetime reached around 500 ps, ideal for fast-imaging applications. The cell studies demonstrated that the NPs do not lower the cell viability below 90 % and can be internalized by different neurological cell types. A clear difference was observed between the uptake of MDMO-PPV NPs and CPM-MDMO-PPV NPs, the latter one being faster due to the surface charge of the carboxylic acid groups indicating the profound effect of an additional surface charge. As the results with the neurological cell lines are very encouraging, these NP systems apart from serving as a useful bioimaging probe will certainly spur new avenues for understanding some of the complex processes at the cellular level within the CNS. The results presented highlight that PPV-derivative based NPs are excellent candidates for bioimaging

applications due to their interesting optical properties, design flexibility for surface functionalization, and benign biological characteristics.

ASSOCIATED CONTENT

Supporting Information. Additional supporting figures and material and methods as described in the article. This material is available at free of charge via the Internet at http://pubs.acs.org.

Additional characterization protocols of synthesized polymers and nanoparticles; molecular weights of synthesized PPVs (Figure S1-2); NMR spectrum of CPM-MDMO-PPV polymer (Figure S3); comparative infrared spectra of both PPV polymers (Figure S4); TEM image of MDMO-PPV NPs (Figure S5); additional EDX-spectrum of CPM-MDMO-PPV NPs functionalized with gold labeled Abs (Figure S6); lifetime measurement data of PPV-based NPs versus reference polystyrene NPs and Rhodamine B (Figure S7); absorbance integrity measurement of PPV NPs over 1 year period and after 24h exposure to 0.1 wt% H_2O_2 (Figure S8-9); MTT and alamar blue cytotoxicity assays for MDMO-PPV NPs in HeLa cells (Figure S10-11); CPM-MDMO-PPV NPs alamar blue cytotoxicity assay on trio of neural cell lines (Figure S12); additional confocal images of PPV NPs in different neurological cell lines and HeLa cells (Figure S13-16).

AUTHOR INFORMATION

Corresponding Author

* E-mail: anitha.ethirajan@uhasselt.be

Notes

The authors declare no competing financial interest.

Author Contributions

The manuscript was written through contributions of all authors. All authors have given approval to the final version of the manuscript.

Funding Sources

The Authors thank the Agency for Innovation by Science and Technology in Flanders (IWT) and BOF UHasselt for funding.

ACKNOWLEDGMENTS

Support for confocal microscopy was given by Prof dr. Marcel Ameloot. Cells were kindly provided by dr. Annelies Bronckaers, drs. Jo Mailleux and dra. Jasmine Vanmol. Technical support was given by Huguette Penxten and Christel Bocken. MP and NZ are grateful for funding from the IWT (Agentschap voor Innovatie door Wetenschap en Technologie). AE is a FWO (Research Foundation Flanders) post-doctoral fellow. TJ is grateful for funding from FWO in the form of an Odysseus grant. Additional support from BELSPO in the form of the interuniversity attraction pole (IAP) program P7/05: Functional Supramolecular Systems is kindly acknowledged.

ABBREVIATIONS

Ab, antibodies; BSA, bovine serum albumin; CNS, central nervous system; CN-PPV, poly[2,5-dicyano-*p*-phenylene vinylene]; CPM-PPV, 2-(5'-methoxycarbonylpentyloxy)-5-methoxy-1,4-phenylenevinylene; $CDCl_3$, deuterated chloroform; $CHCl_3$, chloroform; DAPI, diamidino-2-phenylindole; DCC/DMAP, dicyclohexylcarbodiimide/4-dimethylaminopyridine; *Đ*, dispersity; DLS, dynamic light scattering; DMEM, dulbecco's modified eagle medium; EDC, 1-ethyl-3-(3-dimethylaminopropyl)carbodiimide; EDX, energy-dispersive x-ray; EGF, epidermal growth factor; FACS, fluoresence-activated cell sorting; FCS, fetal calf serum; FITC, fluorescein isothiocyanate; FLIM, fluorescence lifetime imaging microscopy; HC, hydrocortisone; H_2O_2, hydrogen peroxide; IMDM, iscove's modified dulbecco's medium; MDMO-PPV, poly[2-methoxy-5-(3',7'-dimethoxyoctyloxy)-1,4-phenylenevinylene]; MEH-PPV, poly[2-methoxy-5-(2-ethylhexyloxy)-1,4-phenylenevinylene]; M_n, molecular weight; MTT, methylthiazolyldiphenyl-tetrazolium bromide; NPs, nanoparticles; PBS, phosphate buffered saline; PDI, polydispersity indices; PFA, paraformaldehyde; PMT, photomultiplier tube; PPV, poly(*p*-phenylene vinylene); P/S, penicillin/streptomycin; QY, quantum yield; rM-CSF, macrophage colony stimulating factor; SDS, sodium dodecyl sulfate; sulfo-NHS, Sulfo-N-hydroxysulfosuccinimide; TEM, transmission electron microscopy; THF, tetrahydrofuran.

REFERENCES

1. *Visualizing Chemistry: The Progress and Promise of Advanced Chemical Imaging*. Washington (DC): National Academies Press (US): 2006; p 222.

2. Dean, K. M.; Palmer, A. E. *Nat. Chem. Biol.* **2014,** *10* (7), 512-523.

3. *Advanced Fluorescence Reporters in Chemistry and Biology III: Applications in Sensing and Imaging*. Springer: 2011.

4. Pepperkok, R.; Ellenberg, J. *Nat. Rev. Mol. Cell Biol.* **2006,** *7* (9), 690-696.

5. Yildiz, A.; Forkey, J. N.; McKinney, S. A.; Ha, T.; Goldman, Y. E.; Selvin, P. R. *Science* **2003,** *300* (5628), 2061-2065.

6. Xie, X. S.; Yu, J.; Yang, W. Y. *Science* **2006,** *312* (5771), 228-230.

7. Thompson, M. A.; Casolari, J. M.; Badieirostami, M.; Brown, P. O.; Moerner, W. E. *Proc. Natl. Acad. Sci.* **2010,** *107* (42), 17864-17871.

8. Wu, C.; Bull, B.; Szymanski, C.; Christensen, K.; McNeill, J. *ACS Nano* **2008,** *2* (11), 2415-2423.

9. Fernando, L. P.; Kandel, P. K.; Ackroyd, P. C.; Christensen, K. A. *Anal. Bioanal. Chem.* **2012,** *404* (10), 3003-3014.

10. Penjweini, R.; Deville, S.; D'Olieslaeger, L.; Berden, M.; Ameloot, M.; Ethirajan, A. *J. Controlled Release* **2015,** *218*, 82-93.

11. Hofmann, D.; Messerschmidt, C.; Bannwarth, M. B.; Landfester, K.; Mailander, V. *Chem. Commun.* **2014,** *50* (11), 1369-1371.

12. Alford, R.; Simpson, H. M.; Duberman, J.; Hill, G. C.; Ogawa, M.; Regino, C.; Kobayashi, H.; Choyke, P. L. *Molecular imaging* **2009,** *8* (6), 341.

13. Michalet, X.; Pinaud, F. F.; Bentolila, L. A.; Tsay, J. M.; Doose, S.; Li, J. J.; Sundaresan, G.; Wu, A. M.; Gambhir, S. S.; Weiss, S. *Science* **2005,** *307* (5709), 538-544.

14. Bradburne, C. E.; Delehanty, J. B.; Boeneman Gemmill, K.; Mei, B. C.; Mattoussi, H.; Susumu, K.; Blanco-Canosa, J. B.; Dawson, P. E.; Medintz, I. L. *Bioconjugate Chem.* **2013,** *24* (9), 1570-1583.

15. Ahmad Khanbeigi, R.; Abelha, T. F.; Woods, A.; Rastoin, O.; Harvey, R. D.; Jones, M.-C.; Forbes, B.; Green, M. A.; Collins, H.; Dailey, L. A. *Biomacromolecules* **2015,** *16* (3), 733-742.

16. Tuncel, D.; Demir, H. V. *Nanoscale* **2010,** *2* (4), 484-494.

17. Shirakawa, H.; Louis, E. J.; MacDiarmid, A. G.; Chiang, C. K.; Heeger, A. J. *J. Chem. Soc., Chem. Commun.* **1977,** (16), 578-580.

18. Junkers, T.; Vandenbergh, J.; Adriaensens, P.; Lutsen, L.; Vanderzande, D. *Polym. Chem.* **2012,** *3* (2), 275-285.

19. Vandenbergh, J.; Cosemans, I.; Lutsen, L.; Vanderzande, D.; Junkers, T. *Polym. Chem.* **2012,** *3* (7), 1722-1725.

20. van Breemen, A. J. J. M.; Vanderzande, D. J. M.; Adriaensens, P. J.; Gelan, J. M. J. V. *J. Org. Chem.* **1999,** *64* (9), 3106-3112.

21. Zhang, W.; Sun, H.; Yin, S.; Chang, J.; Li, Y.; Guo, X.; Yuan, Z. *J. Mater. Sci.* **2015,** *50* (16), 5571-5577.

22. Xu, J.; Zhou, Y.; Cheng, G.; Liu, S.; Dong, M.; Huang, C. *Luminescence* **2015,** *30* (4), 451-456.

23. Sun, K.; Chen, H.; Wang, L.; Yin, S.; Wang, H.; Xu, G.; Chen, D.; Zhang, X.; Wu, C.; Qin, W. *ACS Appl. Mater. Interfaces* **2014,** *6* (13), 10802-10812.

24. Doshi, M.; Krienke, M.; Khederzadeh, S.; Sanchez, H.; Copik, A.; Oyer, J.; Gesquiere, A. J. *RSC Adv.* **2015,** *5* (47), 37943-37956.

25. Ritz, S.; Schöttler, S.; Kotman, N.; Baier, G.; Musyanovych, A.; Kuharev, J.; Landfester, K.; Schild, H.; Jahn, O.; Tenzer, S.; Mailänder, V. *Biomacromolecules* **2015,** *16* (4), 1311-1321.

26. Tenzer, S.; Docter, D.; Kuharev, J.; Musyanovych, A.; Fetz, V.; Hecht, R.; Schlenk, F.; Fischer, D.; Kiouptsi, K.; Reinhardt, C.; Landfester, K.; Schild, H.; Maskos, M.; Knauer, S. K.; Stauber, R. H. *Nat Nano* **2013,** *8* (10), 772-781.

27. Pecher, J.; Mecking, S. *Chem. Rev.* **2010,** *110* (10), 6260-6279.

28. Landfester, K. *Adv. Mater.* **2001,** *13* (10), 765-768.

29. Ethirajan, A.; Landfester, K. *Chem. - Eur. J.* **2010,** *16* (31), 9398-9412.

30. Ethirajan, A.; Musyanovych, A.; Chuvilin, A.; Landfester, K. *Macromol. Chem. Phys.* **2011,** *212* (9), 915-925.

31. Moreno-Vega, A.-I.; Gomez-Quintero, T.; Nunez-Anita, R.-E.; Acosta-Torres, L.-S.; Castano, V. *J. Nanotechnol.* **2012,** *2012*, 10.

32. Ajetunmobi, A.; Prina-Mello, A.; Volkov, Y.; Corvin, A.; Tropea, D. *Prog. Neurobiol.* **2014,** *123*, 18-36.

33. Qian, C.-G.; Zhu, S.; Feng, P.-J.; Chen, Y.-L.; Yu, J.-C.; Tang, X.; Liu, Y.; Shen, Q.-D. *ACS Appl. Mater. Interfaces* **2015,** *7* (33), 18581-18589.

34. Duchateau, J.; Lutsen, L.; Guedens, W.; Cleij, T. J.; Vanderzande, D. *Polym. Chem.* **2010,** *1* (8), 1313-1322.

35. Zaquen, N.; Vandenbergh, J.; Schneider-Baumann, M.; Lutsen, L.; Vanderzande, D.; Junkers, T. *Polymers* **2015,** *7* (3), 418-452.

36. Van Severen, I.; Motmans, F.; Lutsen, L.; Cleij, T. J.; Vanderzande, D. *Polymer* **2005,** *46* (15), 5466-5475.

37. Deen, C.; Claassen, E.; Gerritse, K.; Zegers, N. D.; Boersma, W. J. A. *J. Immunol. Methods* **1990,** *129* (1), 119-125.

38. Correa-Llantén, D. N.; Muñoz-Ibacache, S. A.; Castro, M. E.; Muñoz, P. A.; Blamey, J. M. *Microb. Cell Fact.* **2013,** *12*, 75-75.

39. Schwartz, B. J. *Annu. Rev. Phys. Chem.* **2003,** *54* (1), 141-172.

40. Howes, P.; Green, M.; Levitt, J.; Suhling, K.; Hughes, M. *J. Am. Chem. Soc.* **2010,** *132* (11), 3989-3996.

41. Nguyen, T.-Q.; Martini, I. B.; Liu, J.; Schwartz, B. J. *J. Phys. Chem. B* **2000,** *104* (2), 237-255.

42. Wu, C.; Szymanski, C.; Cain, Z.; McNeill, J. *J. Am. Chem. Soc.* **2007,** *129* (43), 12904-12905.

43. Denk, W.; Strickler, J.; Webb, W. *Science* **1990,** *248* (4951), 73-76.

44. Pecher, J.; Huber, J.; Winterhalder, M.; Zumbusch, A.; Mecking, S. *Biomacromolecules* **2010,** *11* (10), 2776-2780.

45. Bao, B.; Tao, N.; Yang, D.; Yuwen, L.; Weng, L.; Fan, Q.; Huang, W.; Wang, L. *Chem. Commun.* **2013,** *49* (90), 10623-10625.

46. Resch-Genger, U.; Grabolle, M.; Cavaliere-Jaricot, S.; Nitschke, R.; Nann, T. *Nat. Methods* **2008,** *5* (9), 763-775.

47. Wu, C.; Chiu, D. T. *Angew. Chem., Int. Ed.* **2013,** *52* (11), 3086-3109.

48. Ye, F.; Wu, C.; Jin, Y.; Wang, M.; Chan, Y.-H.; Yu, J.; Sun, W.; Hayden, S.; Chiu, D. T. *Chem. Commun.* **2012,** *48* (12), 1778-1780.

49. Chambon, S.; Rivaton, A.; Gardette, J.-L.; Firon, M.; Lutsen, L. *J. Polym. Sci., Part A: Polym. Chem.* **2007,** *45* (2), 317-331.

50. Jiang, X.; Musyanovych, A.; Röcker, C.; Landfester, K.; Mailänder, V.; Nienhaus, G. U. *Nanoscale* **2011,** *3* (5), 2028-2035.

51. Raff, M.; Abney, E.; Cohen, J.; Lindsay, R.; Noble, M. *J. Neurosci.* **1983,** *3* (6), 1289-1300.

52. An, Y.; Chen, Q.; Quan, N. *J. Inflammation Res.* **2011,** *2011* (4), 11-20.

53. Blasi, E.; Barluzzi, R.; Bocchini, V.; Mazzolla, R.; Bistoni, F. *J. Neuroimmunol.* **1990,** *27* (2), 229-237.

54. Hanisch, U.-K.; Kettenmann, H. *Nat. Neurosci.* **2007,** *10* (11), 1387-1394.

55. Block, M. L.; Zecca, L.; Hong, J.-S. *Nat. Rev. Neurosci.* **2007,** *8* (1), 57-69.

56. Graeber, M. B. *Science* **2010,** *330* (6005), 783-788.

57. Kettenmann, H.; Hanisch, U.-K.; Noda, M.; Verkhratsky, A. *Physiol. Rev.* **2011,** *91* (2), 461-553.

58. Takeuchi, A.; Miyaishi, O.; Kiuchi, K.; Isobe, K.-i. *J. Neurosci. Res.* **2001,** *65* (1), 38-44.

TABLE OF CONTENTS GRAPHIC